Exploration and comparison of inborn capacity of aerobic and anaerobic metabolisms of *Saccharomyces cerevisiae* for microbial electrical current production

Longfei Mao* and Wynand S Verwoerd

Centre for Advanced Computational Solutions; Department of Molecular Biosciences; Lincoln University; Lincoln, New Zealand

Saccharomyces cerevisiae possesses numerous advantageous biological features, such as being robust, easily handled, mostly non-pathogenic and having high catabolic rates, etc., which can be considered as merits for being used as a promising biocatalyst in microbial fuel cells (MFCs) for electricity generation. Previous studies have developed efficient MFC configurations to convert metabolic electron shuttles, such as cytoplasmic NADH, into usable electric current. However, no studies have elucidated the maximum potential of *S. cerevisiae* for current output and the underlying metabolic pathways, resulting from the interaction of thousands of reactions inside the cell during MFC operation. To address these two key issues, this study used in silico metabolic engineering techniques, flux balance analysis (FBA), and flux variability analysis with target flux minimization (FATMIN), to model the metabolic perturbation of *S. cerevisiae* under the MFC-energy extraction. The FBA results showed that, in the cytoplasmic NADH-dependent mediated electron transfer (MET) mode, *S. cerevisiae* had a potential to produce currents at up to 5.781 A/gDW for the anaerobic and 6.193 A/gDW for the aerobic environments. The FATMIN results showed that the aerobic and anaerobic metabolisms are resilient, relying on six and five contributing reactions respectively for high current production. Two reactions, catalyzed by glutamate dehydrogenase (NAD) (EC 1.4.1.3) and methylene tetrahydrofolate dehydrogenase (NAD) (EC 1.5.1.5), were shared in both current-production modes and contributed to over 80% of the identified maximum current outputs. It is also shown that the NADH regeneration was much less energy costly than biomass production rate. Taken together, our finding suggests that S. cerevisiae should receive more research effort for MFC electricity production.

Introduction

Saccharomyces cerevisiae is associated with anthropic environments and is well known for food or beverage (alcoholic) fermentation.[1] Besides these applications, this yeast species has been employed as an eukaryotic model organism in molecular and cell biology; for example, the characteristics of many proteins can be discovered by studying their homologs in *S. cerevisiae*.[2-6] Recently, it has been shown that *S. cerevisiae* can be processed to produce potential advanced biofuels such as long chain alcohols and isoprenoid- and fatty acid-based biofuels, which have physical properties that more closely resemble petroleum-derived fuels.[7] Nevertheless, biofuels need to be further combusted to produce usable energy in the form of electricity. To circumvent the disadvantages of biofuel combustion and directly convert the metabolic reducing potential inside the cell into electricity, another device, named a microbial fuel cell (MFC), has also been proposed. In a typical MFC

configuration, microorganisms are grown in the anodic compartment and obtain electrons from breaking down substrate during growth.[8] The gained electrons can be harnessed and transported out of cells to an electrode via two main operational modes, mediated electron transfer (MET), and direct electron transfer (DET) modes.[8] MET mode involves soluble redox mediators (such as bromocresol green [BG] and neutral red [NR][9]) that act as electron relays repeatedly cycling between the metabolism of the cell and the electrode,[10] whereas DET mode is the case where electrons are directly expelled by some microorganisms via membrane-associated proteins (e.g., *c*-type cytochrome).[10] In either of these modes, the physiological effect of the immersion of a microbe in the anodic compartment is that an electron drain is introduced by the external environment. Because of the key role of redox carriers in most aspects of metabolism, operation of the metabolic network is fundamentally affected by this. The focus of this article is to model the resulting rebalancing of metabolic fluxes by using flux balance

analysis (FBA). Further exposition of the working principle of an MFC can be found in several review articles.[8,11,12]

Both MET and DET modes can be used in MFCs based on *S. cerevisiae*.[11] In the DET mode, the yeast based MFC could so far only produce an extremely low current output, at a scale of microamperes.[13] In addition, it is unclear what mechanisms on the cell wall are responsible for DET current production.[14] In the MET mode, mediators are required to facilitate the transfer of electrons to the anode, because this yeast is thought incapable of producing such mediators indigenously.[15] Because glycolysis occurs in the cytosol of the yeast cell rather than in the mitochondria, the electron shuttle, NADH, is easily accessible to a mediator molecule present in the cell membrane of the yeast and has been proposed as the main electron supplier in a yeast-based MFC.[15,16] Based on these characteristics, MFCs using yeast can be directly applied in fermenters for in situ power generation.[15] Other electron carriers (such as $FADH_2$) may also contribute to current production, but these reduced molecules are regenerated by much fewer reactions than NADH, which is widely used in many reactions of the energy metabolism (e.g., glycolysis and Krebs cycles).

Since the biological entity, *S. cerevisiae*, in the MFCs are considered as the fundamental part that determines the current and power output of MFC and draws a distinction between MFC and other chemical fuel cells, it would be desirable to know the inherent restrictions and mechanisms of the yeast for current generation and to understand how the energy extraction perturbs the metabolic mechanisms of microorganisms in MFCs. Although some studies have discussed the metabolisms for supplying electrons in MFCs based on empirical knowledge of the textbook biochemical pathways or limited results arising from reductionist investigative methods, there is still an urgent demand for knowledge about the metabolic pathways resulting from the interaction of thousands of reactions inside the yeast cell during MFC operation. This task can be solved by in silico modeling of genome-scale metabolic network reconstructions (GENRE), using the recently developed constraint-based modeling approaches.[17,18] However, these novel methods had not been used in MFC research area until recently.[11,19,20]

In this study, to identify the maximum potential of *S. cerevisiae* to sustain the energy extraction process in yeast-based MFCs, FBA, and multi-objective optimization[19,20] was employed to investigate the metabolic capability of the yeast to supply an excess flux of cytosolic NADH to reduce the oxidized mediators (or anode), under two broad metabolic types, anaerobic and aerobic growth. A genome-scale metabolic model of *S. cerevisiae* (yeast 5) was chosen as the backbone for the present flux balance modeling, since it has been tested extensively against experimental results for prediction of several growth conditions, including byproduct synthesis, in a previous study.[21] Only minimal changes were made to the model for our study, to represent the diversion of redox carriers in a MFC. In addition, flux variability analysis with target flux minimization (FATMIN)[20] was implemented to elucidate pertinent reactions underlying the maximum current output. Finally, robustness analysis was conducted to establish the feedstock costs for the cytosolic NADH-linked electricity generation in *S. cerevisiae*.

Results and Discussion

Impact of the redox perturbation on the biomass production. **Figure 1** shows how production of mediated electron transfer (MET) aimed at cytosolic NADH competes with biomass production for metabolic resources. MET influenced the production of the NADH and biomass in the same way for both anaerobic and aerobic conditions, that is, the increase in MET drove the NADH regeneration rates in the two growth modes toward their maximum attainable values, and the corresponding NADH flux consumed for cell maintenance and biomass formation rates toward zero. This indicates most of the energy originally for growth is converted to electricity.

At the base state optimized for growth, the total turnover rate of NADH were 19.74 mmol/gDW/h and 67.34 mmol/gDW/h for the anaerobic and aerobic condition respectively. Compared with the base states, the anaerobic and aerobic metabolisms had a potential to increase their NADH regeneration rates by about 5.469 (447%) and 1.716 (71.6%) folds respectively under the highly NADH-perturbed metabolic states, achieving the highest NADH_mfc flux values of about 108 mmol gDW^{-1} h^{-1} for the anaerobic growth and 115.6 mmol gDW^{-1} h^{-1} for the aerobic growth, which were achievable when biomass production rate was suppressed to 0.012 and 0.01284 h^{-1} in the anaerobic and aerobic modes respectively. This indicates that aerobic respiration can increase the maximum biomass production rate, but does not substantially influence the metabolic capability for NADH regeneration. At the same substrate consumption rate, the fermentation can regenerate NADH to a level that is sufficient to sustain similar electric current output as aerobic growth.

The MET production rates shown in the top parts of **Figure 1** for the two growth cases, only show a linear dependence on biomass growth for small growth rates. Starting from the unperturbed state of zero MET production at the right hand side of the plots and based on the slope changes in the lines connecting two neighboring data points, the relationships between varying biomass production rate and the MET (NADH_mfc) rate can be divided into three stages (see **Fig. 1**). These are: an increase in MET without changing biomass growth (Stage I), a downward curving nonlinear rise of MET vs. growth rates (Stage II), and a linear dependence of the rise in MET on drop in biomass formation (Stage III). Stage III only appears in the left corner of the figures, where the line connecting the points clustered indicates there is a linear relationship between the biomass production and the current output.

The slope of the NADH production vs. biomass growth curve as in **Figure 1** gives a direct measure of the efficiency of the underlying pathways. A large slope means that NADH production increases by a large amount for a given cost in terms of biomass production and is therefore highly efficient and vice versa. In the discussions below, we base interpretations of reallocations
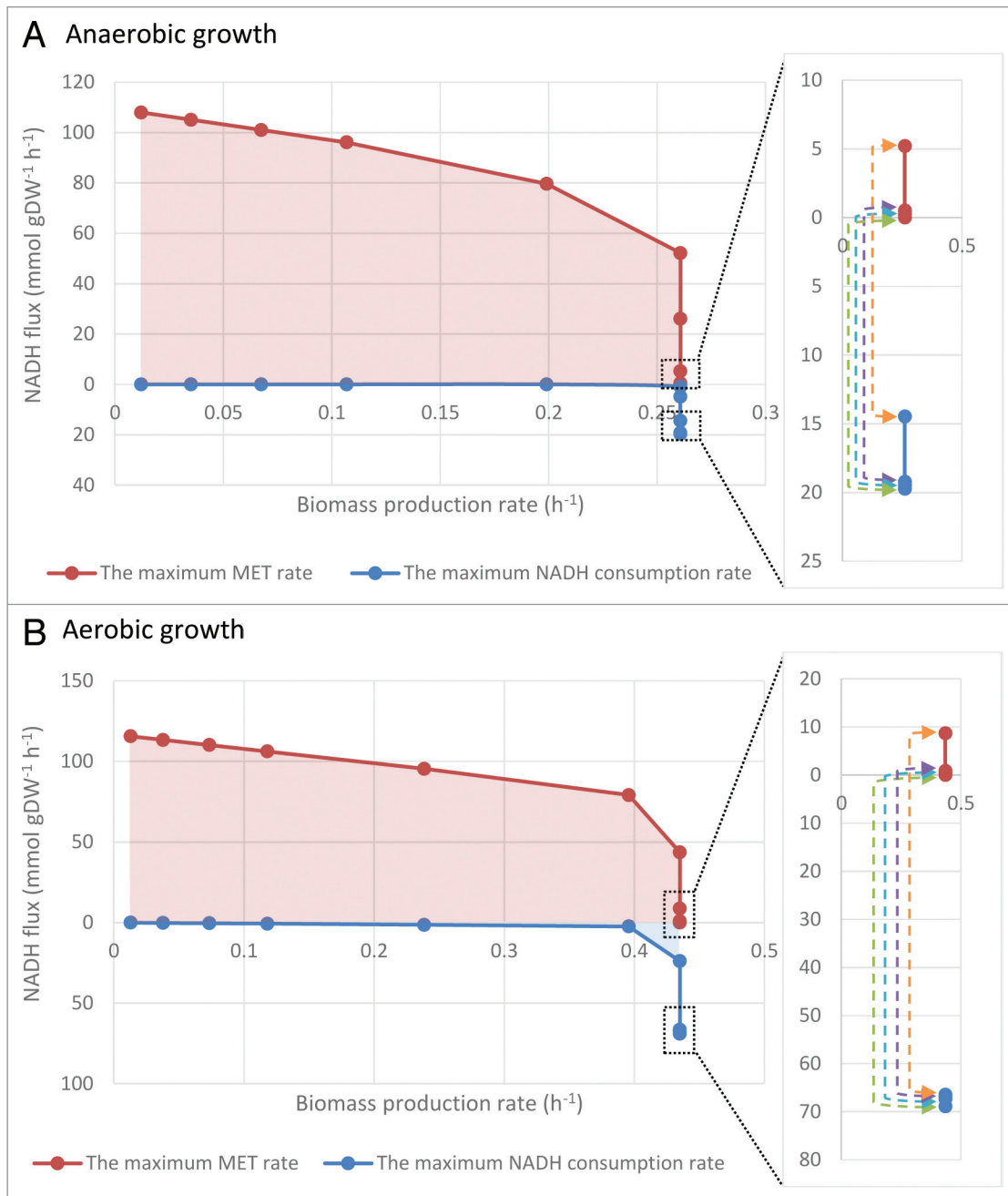
Figure 1. The relationships of the biomass production rate and cytosolic NADH flux diverted toward anode (NADH_mfc). The NADH supplying rate in the MET mode and the reducing equivalent consumption rate for cellular use, as functions of biomass production rate. The red line represents the maximal NADH_mfc flux for a feasible biomass production rate, while any point within the pink area represents all allowable NADH_mfc and biomass production rates. The blue area represents the total cytosolic NADH consuming flux for normal cellular function. The distance between the two lines across the pink and blue areas represents the total available reducing equivalent flux in the cell at a metabolic state related to a specific biomass production rate; inset, enlargement of boxed area. Dashed line with arrowheads indicates which two data points are paired up. The points are simulated by bi-objective optimization involving varying coefficients (λ) assigned for the growth and MET maximizations. A more detailed discussion of the significance of the λ is given in the Methods section. Briefly, it is a parameter that continuously adjusts the metabolic state of the cell through a range stretching from pure growth without the extraction of current (at one extreme) to at state in which all metabolic resources are taken up by supplying electric current and no growth, at the other extreme.

of metabolic resources to pathways with different efficiencies on this evidence directly derived from the modeling results.

Looking at the net NADH production (MET) curve, the Stage I relationship indicates that solutions that are based on

reallocation of energy resources inside cells can elevate the slight increase in MET rate, which obviate the degradation of the intrinsic biological objective, to grow. However, rerouting the energy flow through different metabolic pathways could quell

some cellular functions, which, for example, are unnecessary in optimal growth conditions, but may be important to survival in adverse conditions. This also implies that maximization of growth rate is not the sole goal for eukaryote.

The Stage II indicates that the metabolic pathways have different efficiencies and capability in NADH regeneration. Some pathways possess higher efficiencies in converting the metabolic resource into NADH but lower maximum capability in turnover rate and some others vice versa. When the current output was relatively low, the routes with higher efficiencies were selected to minimize the metabolic resource cost in order to maximize growth rate. When the current output rose to a higher level, those pathways with lower efficiencies but higher upper bounds of the NADH flux had to be used instead.

The Stage III behavior begins at very low growth rate values (less than about 10% of the highest growth rates) in each of the two modes. The Stage III results from the fact that, only a certain set of pathways are able to sustain the very high current output and the flux through these pathways are linearly proportional to current output and biomass production rate.

Figure 1 also shows that a rising MET production rate reduce the cytosolic NADH consumption rate until it finally reaches zero, which indicates that no cytosolic NADH fluxes were consumed for cell maintenance. The curve plotted for the NADH consumption rate vs. the biomass production can be classified into three types: Type I is a reduction in the NADH consumption rate without changing the biomass production rate; Type II represents a decrease in the NADH consumed for maintenance, associated with a drop in biomass production rate; Type III is the phenomenon that (nearly) no cytosolic NADH flux was consumed for cell maintenance accompanied by a decline in the biomass production.

A correspondence can be found between the types of consumption behaviors and the stages displayed by the MET production curves. Stage I coincides with Type I, which is reflected by the observation that the increase in the MET is accompanied by a drop in the NADH consumption for cellular maintenance. This indicates that decreasing NADH flux for internal use would be the primary mechanism implemented by the yeast to relieve the redox perturbation. The similar mechanism has also been seen for the NADH-targeted MET mode of *C. reinhardtii*.[22] This suggests that excess cytosolic NADH may be a common occurrence in eukaryotic microorganisms.

The Stage II occurs with both Type II and III. This indicates that in Stage II, there is a continuous adjustment in the metabolic strategies underlying the MET current production. The reduction in NADH consumption for maintenance may contribute to the major portion of the elevated NADH flux diverted to the mediator in MFCs in the beginning (i.e., the metabolic states undergoing a relatively lower degree of the current-producing perturbation). As the NADH flux shunt further augments, the intracellular pathways that consume cytosolic NADH are disfavored by the metabolism. The cell opts for metabolic pathways that can excessively produce NADH flux for oxidized mediators, while trying to maximize biomass production rate. When entering Stage III of the MET, the cell redirects nearly all of the metabolic resource to NADH regeneration pathways that can supply a high flux of NADH.

Both Stage I and Type I behaviors occurred in the cases of *C. reinhardtii*[22] and *S. cerevisiae*. The coincidence indicates that the multiplicity of eukaryotic functions make these two microorganisms tolerable to hostile situations, since it is originally reflected that there are more routes of energy flow underlying more physiological conditions. In addition, different from *C. reinhardtii*, where the shape of cytosolic NADH consumption line changed in a complex manner, the two cases of *S. cerevisiae* is much simpler. This discrepancy may be a result of the photosynthesis which contains a number of energy pathways providing metabolic fuel to the cell growth.

To further elucidate which one of the two growth conditions can better cope with the NADH-related perturbation, we performed fractional benefit analysis, which calculated a measure called the fractional benefit B as discussed in the methods section. Briefly, B is the sum of the fractions of maximal growth and NADH production respectively, achieved in a particular metabolic state. **Figure 2** shows the result of this measure applied to the reported simulations. Starting from wild type growth rates (right hand side of the figures), an increase in B values can be seen for the Stage I and Type I behavior. The apex points of the B value curves correspond to the highest achievable combined benefit. The maximum B value for the anaerobic growth is a little bit higher than that for the aerobic growth. This suggests that, even though the aerobic growth has a potential to funnel more excess NADH for current production than the anaerobic condition, but the loss of NADH can cause more adverse effects on the aerobic than the anaerobic growth. Both growth conditions can yield a maximum B value of above 75%, which is much higher than those of all other three microorganisms (*G. sulfurreducens*, *C. reinhardtii*, and *Synechocysti*s sp. PCC 6803) that we studied previously.[19,20,22] This indicates that additional NADH perturbations would result in less hostile effects on *S. cerevisiae* than the other three microorganisms and thus *S. cerevisiae* has the greatest suitability for current production among the four.

The metabolic strategies supporting the high NADH regeneration rate in the anaerobic and aerobic modes are elucidated in the next section.

Metabolic strategies for increasing flux of reducing equivalents. A list of identified reactions (enzymes) that were responsible for the promoted diversion of the cytosolic NADH flux toward current production is summarized in **Table 1**.

Anaerobic growth. In the anaerobic fermentation, *S. cerevisiae* relied on six reactions to regenerate NADH from NAD+ at the high rate, subject to the stoichiometry and biological constraints applied. Two of six NADH production routes, namely glutamate dehydrogenase (NAD) (EC: 1.4.1.3) and methylenetetrahydrofolate dehydrogenase (NAD) (EC: 1.5.1.5), were the main NADH suppliers. The two enzyme catalyzed reactions were capable of producing up to 77.48% (85.37 mmol/gDW/h) and 81.23% (85.37 mmol/gDW/h) respectively of the maximum net NADH supplying rate (105.1 mmol/gDW/h). Nevertheless, only the combined fluxes of these two reactions that made up any

percentages within a range of 99.4 to 103.8% of the maximum net NADH flux were viable. This indicates there are unlimited metabolic states that can achieve the FBA identified maximum net NADH shunt. The overflow (the percentage above 100%) can be offset by the consuming NADH fluxes, for instance, the glutamate dehydrogenase (NAD) catalyzed reaction can be reversible and consume up to 3.948 (3.757%) of the maximum net NADH flux.

Another significant portion (22.47%) of the maximum net NADH flux was supplied by four reactions, catalyzed by alcohol dehydrogenase (ethanol to acetaldehyde) (EC: 1.1.1.1), formate dehydrogenase (EC: 1.2.1.2), glyceraldehyde-3-phosphate dehydrogenase (EC: 1.2.1.12), and phosphoglycerate dehydrogenase (EC: 1.1.1.95), respectively. These four reactions had rigid flux values, which accounted for 5.76%, 7.20%, 5.89%, and 3.62% of the maximum net NADH flux respectively. This indicates that they are essential to growth.

All other NADH producing reactions jointly contributed up to only 0.06% of the maximum net NADH flux. This suggests that, in order to achieve a surplus NADH flux of 105.1 mmol/gDW/h, nearly all of the metabolic resources need to be reallocated toward the four aforementioned reactions. In addition, the rigid variability ($v_{i\,min}/v_{i\,max} > 0.99$) of these reaction fluxes under high current output indicates that these reactions were much preferred for the biomass growth, rather than NADH-targeted current production.

Furthermore, it was found that the flux through the reaction catalyzed by alcohol dehydrogenase (EC: 1.1.1.1) merely had a flux of 6.049 mmol/gDW/h under the high degree of NADH perturbation. This is contrary to a previous reporting where alcohol dehydrogenase was suggested as the main NADH sink for mediators.[15]

Conventionally, glycolysis, TCA cycle and fatty acid oxidation are considered to be the three main pathways supplying NADH to oxidative phosphorylation for ATP generation.[23] Consequently, it would be appropriate to speculate that these three pathways are the potential NADH suppliers for mediators in the MFC. However, the presently computed metabolic flux model elucidate that the three pathways for NADH regeneration are not the metabolic pathways responsible for the excess NADH regeneration, subject to the stoichiometry and substrate uptake constraints. Instead, two reactions (EC: 1.4.1.3) in nitrogen metabolism and (EC: 1.5.1.5) in folate biosynthesis are the only two routes allowing a high NADH regeneration rate.

Aerobic growth. Under aerobic respiration, five reactions were identified to have a capability to replenish the loss of cytosolic NADH under high current output. Each of the two reactions, catalyzed by glutamate dehydrogenase (NAD) (EC: 1.4.1.3) and methylene tetrahydrofolate dehydrogenase (NAD) (EC: 1.5.1.5), had a potential to solely supply up to 81.71% of the maximum net NADH flux (113.31 mmol/gDW/h); and any combinations of the reaction flux amount to 81.71–81.75% of the maximum net NADH flux were attainable.

About 18.06% of the maximum net NADH flux was supplied by alcohol dehydrogenase (EC: 1.1.1.90), glyceraldehyde-3-phosphate dehydrogenase (EC: 1.2.1.12), and malate dehydrogenase
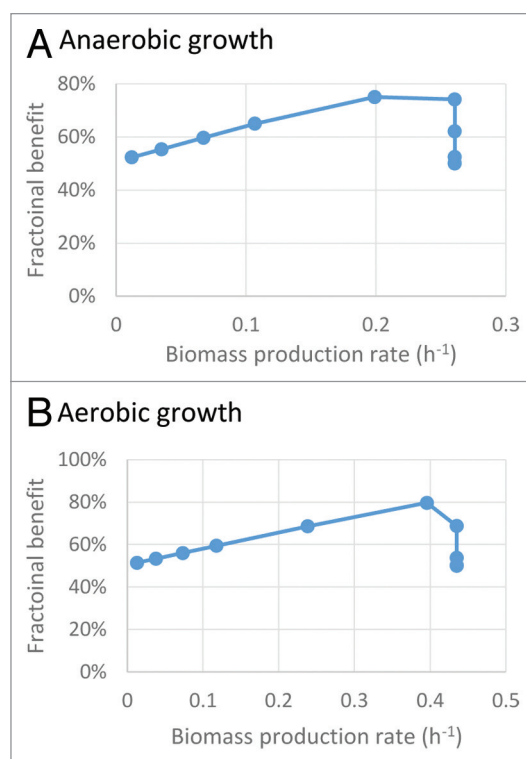

Figure 2. The effect of varying biomass production on the fractional benefit. The fractional benefit B plotted on the vertical axis, is a measure of success in achieving the combined goals of maximal growth rate and MET flux. Maximizing one of these at a time, as at the endpoints, gives only B = 50%. The graphs show that relative to this, gains in MET flux can more than offset losses of growth rate in *S. cerevisiae* metabolism.

(EC: 1.1.1.85). These three reactions had fixed fluxes, implying their enzymatic activities were critical to cell growth.

Comparison of the identified reactions chosen by anaerobic and aerobic growths shows that three reactions, glutamate dehydrogenase (NAD) (EC: 1.4.1.3), glyceraldehyde-3-phosphate dehydrogenase (EC: 1.2.1.12), and methylenetetrahydrofolate dehydrogenase (NAD) (EC: 1.5.1.5), were used by the two modes to achieve a high NADH regeneration rate. This indicates that 87.70% of the maximum net NADH flux in the anaerobic mode and 85.50% of the maximum flux in the aerobic mode were generated through the same pathways.

To demonstrate how nutrient uptake is channeled to biomass growth and current yield respectively, **Table 2** compares the corresponding fluxes at different glucose uptake rates.

Effect of varying glucose uptake rate on predicted biomass and NADH production rates. **Table 2** summarizes the linear functions obtained for biomass and NADH_mfc production rates vs. glucose uptake rates. Column 3 shows that the optimal glucose-to-biomass efficiency was heavily suppressed under the high current output condition in both anaerobic and aerobic growth.

The linear regression equations are first in units (gDW/gDW/h) (column 4) for comparison with the biomass rate and then in the standard flux units (mmol/gDW/h) in column 5.

Table 1. Identified reactions that contribute significantly to the predicted maximum NADH production rate. The flux ranges were calculated from the FATMIN extension of FVA

Reaction ID	NADH flux (mmol/gDW/h)		Enzyme	EC No.	Reaction	Subsystems
	Min	**Max**				
(A) Anaerobic growth						
r_0163	6.049	6.049	alcohol dehydrogenase (ethanol to acetaldehyde)	1.1.1.1	NAD + ethanol < = > NADH + acetaldehyde	Pyruvate metabolism
r_0445	7.566	7.566	formate dehydrogenase	1.2.1.2	NAD + formate = > CO2 + NADH	Methane metabolism
r_0470	–3.948	81.42	glutamate dehydrogenase (NAD)	1.4.1.3	L-glutamate + NAD < = > 2-oxoglutarate + NADH + NH3	Glutamate metabolism (aminosugars metabolism)
r_0486	6.186	6.186	glyceraldehyde-3-phosphate dehydrogenase	1.2.1.12	D-glyceraldehyde 3-phosphate + NAD + phosphate < = > 3-phospho-D-glyceroyl phosphate + NADH	Glycolysis/Gluconeogenesis
r_0731	0	85.37	methylenetetrahydrofolate dehydrogenase (NAD)	1.5.1.5	5,10-methylenetetrahydrofolate + NAD < = > 5,10-methenyltetrahydrofolate + NADH	One carbon pool by folate
r_0891	3.808	3.808	phosphoglycerate dehydrogenase	1.1.1.95	3-phospho-D-glycerate + NAD = > 3-phospho-nooxypyruvate + NADH	Glycine, serine and threonine metabolism
(B) Aerobic growth						
r_0163	9.971	9.971	alcohol dehydrogenase (ethanol to acetaldehyde)	1.1.1.1	NAD + ethanol < = > NADH + acetaldehyde	Pyruvate metabolism
r_0470	–0.2163	92.58	glutamate dehydrogenase (NAD)	1.4.1.3	L-glutamate + NAD < = > 2-oxoglutarate + NADH + NH3	Glutamate metabolism (aminosugars metabolism)
r_0486	4.303	4.303	glyceraldehyde-3-phosphate dehydrogenase	1.2.1.12	D-glyceraldehyde 3-phosphate + NAD + phosphate < = > 3-phospho-D-glyceroyl phosphate + NADH	Glycolysis/Gluconeogenesis
r_0714	6.190	6.190	malate dehydrogenase, cytoplasmic	1.1.1.85	2-isopropylmalate + NAD < = > 4-methyl-2-oxopentanoate + CO2 + NADH	Branched chain amino acid metabolism (valine, leucine and isoleucine)
r_0731	0	92.58	methylenetetrahydrofolate dehydrogenase (NAD)	1.5.1.5	5,10-methylenetetrahydrofolate + NAD < = > 5,10-methenyltetrahydrofolate + NADH	One carbon pool by folate

Note: see the supplementary file for the FATMIN results of all the reactions involving NADH and list of the metabolite and reaction abbreviations.

Comparison of columns 3 and 4 indicates that NADH regeneration is much less substrate-costly than the biomass production.

Compared with anaerobic growth, the efficiency of conversion of glucose to biomass was 66.67% higher, but the efficiency for glucose to NADH was just 7.831% higher in the aerobic growth. This implies that the intake of oxygen can promote the biomass production but has fewer effects on NADH regeneration.

Finally, the two operation modes are compared for their theoretically maximum current output in **Figure 3** and **Table 3**.

Comparison of amperage outputs. Overall, the maximum current output achieved for aerobic growth (6.193 A/gDW) was about 7.14% higher than for its anaerobic counterpart (5.781 A/gDW). Since aerobic metabolism can more efficiently use substrate than the anaerobic, aerobic MFCs were expected to be capable of generating more current that the anaerobic one. This anticipation is in keeping with the present study's prediction, despite the common observation that fuel cells generate less current when they were supplied with substrate (or anolyte) containing oxygen.[24] The discrepancy between expectations and reality may be ascribed to the deficiency of the engineering design that allows the reduced mediators to be intercepted by the presence of oxygen rather than anode, resulting in low observed coulombic efficiency. Although fermentation produces a lower current than oxidative phosphorylation, anaerobic growth eliminates the need to aerate large volumes of media and thus is more suitable for application in large-scale MFC.

In general, yeast based MFCs perform better than cyanobacteria but still have a lower power output than bacterial fuel cells.[25] An experimentally observed current of 16.09 ± 8 μA was recorded when the cell was operating under its lowest impedance in a previous *S. cerevisiae* based MFC.[15] The anode solution contained 2 g of the yeast, and thus the aforementioned amperage output of the MFC system can be converted into 8.45 ± 4 μA/g DW, which is much lower than the maximum current output (5.714 A/g) computed for anaerobic growth in the present study. Another experimental study of a methylene blue mediated *S. cerevisiae* MFC reported a maximum current output of 3 mA.[26] With the cell density of 50 mg/mL and anode volume of 10 mL provided

in the same study, a 0.006A/g can be calculated,[26] which is still much lower than the presently computed value (5.714 A/g). The large discrepancy between the previously reported current per cell gram and the presently computed one may be attributed to the fact that (1) the cells were not in optimal metabolic states, (2) not every single cell participated in current output, (3) the mediator, i.e., methylene blue (MB), could not penetrate the cell wall and/or cytoplasmic membrane, and thus could not interact with the cytoplasmic metabolic activity efficiently, (4) and the engineering design might not efficiently collect all the electrons funneled away from the microorganism.

The eukaryotic respiratory chain has a complicated architecture which is advantageous to the cell energy balance.[27] The cell membrane contains higher protein content, which corresponds to the higher rate of redox reactions between cytoplasm and inter-membranous space.[27] This feature has been proposed to facilitate *S. cerevisiae* attached to the anode to convey electrons to the electric circuit without aids of artificial mediators in an MFC.[16] The intracellular redox mediators (i.e., NAD⁺/NADH and FAD⁺/FADH) were suggested to sustain a current output of up to 282.83 mA/m.[2,16] However, without knowledge of the cell density on the anode of the MFC, it is impossible convert the unit (mA/m^2) of the reported current density into a unit of amperage per gram dry weight cell, and therefore we are unable to compare the current output of the yeast cell in this particular MFC to the theoretical maximum value computed here.

Another more recent study investigated the possibility of *S. cerevisiae* to transfer electrons to an extracellular electron acceptor through DET mode and found that the cells adhered to the anode were able to sustain power generation in a mediator-less MFC configuration. It is proposed that the surface confined species are responsible for the DET,[14] however, the power performance of this MFC was extremely low (0.003 W m^{-2} and 0.03 A/m^2).[14] With a reported cell sample weight of 0.13 g and the anode surface area of 4 cm^2, the current density can be translated into 0.000009231A/g. Since the DET mode is based on surface confined species and it is unclear what those species are, identification of the protein involved in such a DET mode is required, before the in silico method presented in this study can be employed to reveal the innate capability of the DET mode based on *S. cerevisiae*.

Conclusions

In this study, the anaerobic and aerobic growth modes of *S. cerevisiae* were modeled to study its maximum potential for MFC current output and underlying metabolic metabolisms. It was shown that a similar level of maximum current outputs can be achieved for the two growth modes (i.e., 5.781 A/gDW for the anaerobic growth and 6.193 A/gDW for the aerobic growth), whereas under aerobic conditions the yeast achieved nearly twice the anaerobic growth rate. To achieve the highest efficiency of NADH regeneration and maximize the current output, the aerobic and anaerobic metabolisms relied on two reactions, catalyzed by glutamate dehydrogenase (NAD) (EC 1.4.1.3) and methylene tetrahydrofolate dehydrogenase (NAD) (EC 1.5.1.5), for NADH
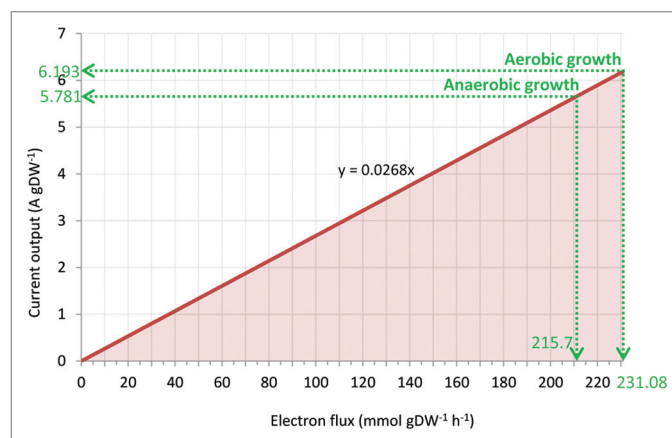

Figure 3. The current output (A/g) as a function of electron flux. The dark red line denotes the maximal current outputs and NADH_mfc production rate, while the area represents all allowable current outputs and electron production rates. The round dotted arrow line indicates the maximal current output and corresponding electron production rate when the growth rate is set to 5% of the predicted maximum growth rate (0.01303 h^{-1}).

production. Besides, the robustness analysis indicated that the NADH regeneration was much less energy costly than the biomass production rate. Taken together, our findings suggest that *S. cerevisiae* should be re-evaluated and receive more research effort for MFC electricity generation.

Materials and Methods

General modeling assumptions. The modeling was conducted based on the three assumed conditions: (1) The MFC reactor is a chemostat that can provide all the necessary nutrients to maintain the optimal microbial growth; (2) Only a pure *S. cerevisiae* culture is used for electricity generation; (3) A putative ideal mediator (e.g., Neutral red[28]) can be found to enter the cytoplasm, intercept the electrons from NADH-involved metabolic activity and convey the electrons to the anode; and (4) The uptake rate of the organic substrate (i.e., glucose) is allowed to vary but is constrained to a realistic range to reflect the observed uptake rates for optimal growth.

Modeling electrode interactions. The interactions with an electrode were captured by introducing two reactions into the model reconstruction (**Table 4**). These reactions represent the net reaction between the reducing equivalents and the electrodes in the MFC.

The two added reactions reflect a well-established understanding[29] that mediators in an MFC enter the cell and interact with cytosolic NADH in the metabolism to extract energy (in the form of electrons) from these electron shuttles, as schematically shown in **Figure 4**. Because NADH is a major electron carrier in microbial metabolism connecting many different cellular processes, known as a "hub" in terms of network theory,[30] the effects of the NADH drain that the added reactions creates, propagates throughout the metabolic network. In this way, the modeling can estimate the maximum power achievable for a microorganism in

Table 2. The summary of linear functions of the biomass production and MET rates in the heterotrophic, photoautotrophic, and mixotrophic modes

Metabolic type	Substrate	Growth (gDW/gDW/h)	MET	
			(gDW/gDW/h)	**(mmol/gDW/h)**
Anaerobic	glucose	$y_c = 0.0261x$	$y_{(g/gDW/h)} = 6.971x$	$y_{(mmol/gDW/h)} = 10.509x$
		$y_p = 0.0035x$		
Aerobic		$y_c = 0.0435x$	$y_{(g/gDW/h)} = 7.518x$	$y_{(mmol/gDW/h)} = 11.332x$
		$y_p = 0.0038x$		

Note: The FBA simulations were performed by changing the photon uptake rate and the glucose uptake rate with the maximization of the objectives. y denotes the MET rate (mmol/gDW/h or gDW/gDW/h) or growth rate (gDW/gDW/h), whereas x represents the substrate (i.e., glucose) uptake rates (mmol/gDW/h). y_c represents the optimal growth, whereas y_p denotes The perturbed growth under cytosolic NADH deprivation.

Table 3. Comparison of predicted amperage output under theoretical maximum current output condition and 5% of optimal growth rate condition

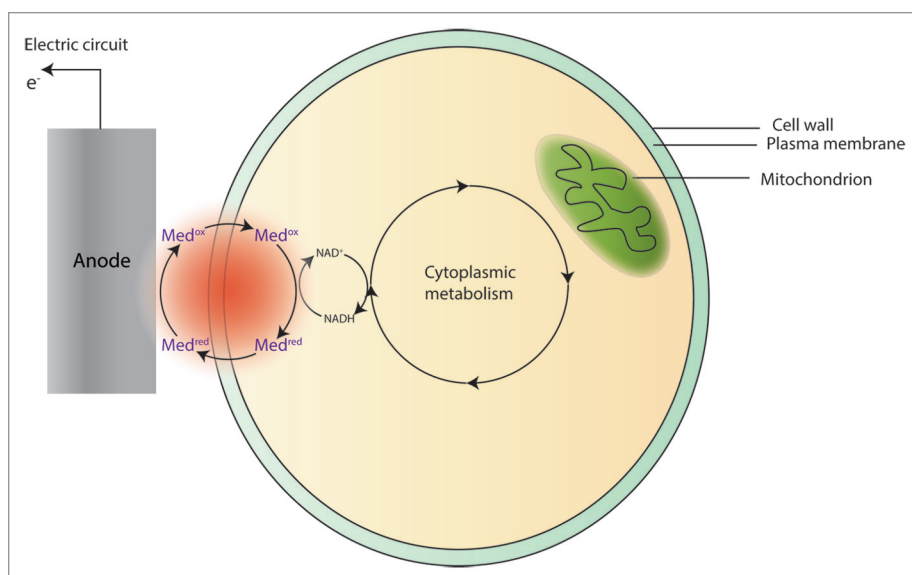| Mode	Conditions	Biomass production rate (h^{-1})	Electron (mmol gDW^{-1} h^{-1})	Amperage (A gDW^{-1})	Coulombic efficiency (CE%)	W gDW^{-1}
Anaerobic	5% of optimal growth rate	0.01303	215.7	5.781	89.87%	4.798
Aerobic			231.1	6.193	96.29%	5.141

Figure 4. A schematic of the modeled anodic mechanisms where the cytoplasmic NAD$^+$/NADH cycle as the electron supplier. Microbes take up substrates (glucose) generating carbon dioxide and proton. This process yield electrons for metabolic benefit, i.e., growth, and reduces Med$_{ox}$ in the cytosol into Med$_{red}$. Med$_{red}$ diffuses into contact with the electrode, where Med$_{red}$ reduces the electrode generating electrical current. The oxidized form, Med$_{ox}$, diffuses back through anolyte for reuse by the microbes. The radial red circle highlights the redox cycle supplying the electron to the anode, which is investigated in the present modeling.

maximization of the production of an overflow flux of desirable reducing equivalent, cytoplasmic NADH, so as to restore the redox balance perturbed by the energy extraction process during MFC operation. The bi-level objective optimization can result in a set of Pareto-optimal points,[37] forming a Pareto front, which describes the trade-off relationship between the growth rate of the organism and the regeneration rate of a plethora NADH flux. Through varying the relative weights associated with each objective,[38] the impact of the enhanced energy extraction on the growth of the cell can be evaluated. The bi-objective equation in this study is defined as follows in terms of the biomass growth flux F_B and the reducing equivalent diversion flux F_N:

$$O = (1 - \lambda) F_B + \lambda g F_N$$

A unit conversion factor g is explicitly provided because in the model, F_N and F_B are measured respectively in units (mmol/gDW/h and g/gDW/h or [h^{-1}]). This ensures that λ is a dimensionless fraction that can be directly interpreted as the relative contribution of the NADH flux to the combined objective.

Fractional benefit analysis. The bi-objective optimization conducted in this study can assess how metabolic energy loss during current production influences the biomass growth. However, the mathematical optimization method based on such a bi-objective function cannot clarify the combined benefit resulting from an optimized metabolic state. Therefore, this requires implementation of fractional benefit analysis to mathematically quantify either extreme on the Pareto front; even though only one of the

MFC, as well as elucidate the response of energy metabolism to the perturbation induced by electricity generation.

Objective equation. The objective equation was formulated as described in our recent studies.[19,22] Briefly, we constructed a bi-objective equation that comprises two objectives: one is the maximization of the growth rate, which reflects the belief that microbes evolve to optimize their metabolisms for maximizing biomass production (growth rate)[31-34] and has been experimentally validated by numerous studies[32,35,36]; the other is the

objective terms is maximized, the other term also has a value and will contribute (positively or negatively) to the overall benefit. In the fractional benefit analysis, each of F_B and F_N is scaled as a fraction of the maximal values F_B^* and F_N^* they can ever achieve, i.e., the values when each is independently maximized. As the maximum of each of these fractions is 1, a plausible measure of the combined benefit achieved in any particular metabolic state is the value of the quantity we denote as the fractional benefit B:

$$B = \frac{1}{2}\left(\frac{F_N}{F_N^*} + \frac{F_N}{F_N^*} \right)$$

A value of B in excess of 50%, indicates that gains in one objective more than compensates for losses in the competing objective.

Conversion of units of flux and current. Current (in amperes) was integrated over time and converted to electrons recovered by using the following conversions: 1 C = 1 A × 1 s, 1 C = 6.24 × 10^{18} electrons, and 1 mol = 6.02 × 10^{23} electrons (the Faraday constant 96485 C/mol). Therefore, one flux unit (mmol/g/h) can be converted into A/g as follows:

$$1 \text{ mmol/g/h} = \frac{1 \text{ mol}}{1000\text{g} \times 3600\text{s}} \times \frac{96485 \text{ C}}{\text{mol}} = 0.0268 \text{ A/g}$$

Calculation of Coulombic efficiency (CE). One of the parameters commonly used to quantify the performance of MFCs is the Coulombic efficiency (CE). The CE is defined as the ratio of electrons transferred to the anode to that in the starting substrate. We use the full oxidation of glucose with oxygen as the oxidant as the reference reaction to characterize the energy efficiency of the respiratory metabolism:

Glucose oxidation reaction: $C_6H_{12}O_6 + 6 H_2O \rightarrow 6 CO_2 + 24 H^+ + 24 e^-$

Based on such stoichiometric information, 1 mol of glucose supplies 24 mol of electrons.[39]

$$\text{CE\%} = \frac{C_{output}}{C_{substrate}} \times 100\% = \frac{\text{The MET flux(mmol/gDW/h)} \times 100}{\text{acetate uptake rate (mmol/gDW/h)} \times 24}\%$$

Calculation of theoretical power outputs of the three tested modes. An upper limit for the cell voltage is calculated in this work based on formal potentials of the biological and electrochemical redox processes, as given by:

$$\Delta E_{cell}^{\circ\prime} = E_{cathode}^{\circ\prime} - E_{anode}^{\circ\prime}$$

Here, $\Delta E_{cell}^{\circ\prime}$ is the standard cell potential (aka., electromotive force); $E_{cathode}^{\circ\prime}$ is the standard potential of cathode oxidation; $E_{anode}^{\circ\prime}$ is the standard potential of anode reduction. The formal potentials of the anode and cathode used for calculation of power density in the three operation modes are summarized in **Table 5**.

The real potential derived from the MFC will be reduced due to various potential losses[12] associated with MFC operation, such as ohmic resistances, concentration polarization and kinetic

Table 4. The added reactions for modeling the interaction of the microorganism and the electrode in MFCs

Operation mode of the MFC	Reaction ID	Reaction
MET	1NADHmfc	nadh → nadh_mfc
	2NADHmfc	nadh_mfc → nad + h_emm

nadh_mfc: the NADH available for MET mode of MFCs;
h_emm: the H ions as the by-product released from the reaction 2NADHmfc;

Table 5. The standard potential of the redox reactions involving the electron donor and acceptor for the MFC (measured at pH 7).

		Redox couple	$E^{\circ\prime}$ (V)
Anode	MET	$NAD^+ + H^+ + 2e^- \rightarrow NADH$	−0.320[47]
Cathode		$O_2 + 4H^+ + 4e^- \rightarrow 2H_2O$	+0.51[48-50]

Table 6. The theoretical limit of standard anode potentials of MFC based on *S. cerevisiae*

Electron transfer mode	$E_{anode}^{\circ\prime}$	$E_{cathode}^{\circ\prime}$	$\Delta E_{cell}^{\circ\prime}$
MET	−0.32	0.51	0.83

constraints. These are not taken into account in the calculations reported here.

The MFC standard cell potential calculated as above and shown in (**Table 6**) shows that as long as the same electron donors are used, the choice of biocatalysts will have little effect in the cell potential.

Calculation of the viable growth rate. To obtain a realistic upper value for the current that can be extracted from a microbe, we chose 5% of the maximum theoretical biomass production rate as the minimum viable growth rate. This percentage value is more likely to be achievable in practice, when compared with 1% assumed as the viability threshold for computational identification of the lowest growth rate in several previous studies.[40,41]

Simulating *S. serevisiae* growth. A recently published metabolic network of *S. cerevisieae*, Yeast 5 GEM[21] (Version 5.40; November 2012), was chosen as the analysis backbone for the all the simulations. Compared with previous metabolic networks of this yeast, this network model is a fully compartmentalized and elementally-balanced *S. cerevisiae* metabolic network, which includes more genes and reactions based on genomic, biochemical and physiological information. The details of existing reactions (substrate and cofactor specificity, reaction reversibility, and compartmentalization) in the network have also been re-evaluated to update the model based on existing literature. Furthermore, the SBML file compatible for computation with the COBRA toolbox is attached to the publication.[42]

All simulations were performed on glucose as the sole carbon source. The exchange of ammonium, protons, iron(2+), phosphate, potassium, sodium, sulfate, and water were all unconstrained. The maximum rate of the glucose uptake is set to

10 mmol/gDW/h.[43] For aerobic growth, oxygen exchange was unconstrained.[21] For simulation of anaerobic growth, the oxygen exchange reaction was constrained to 0. In addition, ergosterol, lanosterol, zymosterol, and phosphatidate were allowed for free exchange and the biomass definition was modified by removing 14-demethyllanosterol and ergosta-5,7,22,24(28)-tetraen-3beta-ol from the "lipid" definition.[21] These steps were applied to reflect the observation that yeasts require sterols and fatty acids when cultured under rigidly anaerobic conditions.[21]

Analysis technique. The growth rates and electron production were computationally determined using Flux Balance Analysis (FBA).[44,45] Computations were performed with COBRA Toolbox[42] in MATLAB (The Math-Works Inc) and OptFlux.[46] Flux variability analysis with target flux minimization (FATMIN)[20] was conducted to determine the flux ranges of the reactions in the network under the metabolic states heavily perturbed by electricity generation. FATMIN can examine the feasible flux ranges of the desired reactions (such as NADH-involved ones) of a genome-scale metabolic network, while eliminating the pointlessly high fluxes values of the loop reactions, to achieve biologically meaningful values.

The underlying idea of FATMIN is to collect the fluxes of all reactions that produce the target metabolite (as opposed to those that consume it) and minimize this collective flux while leaving the value of the objective function unchanged. In this way, the flux in reactions that contribute both productive and futile flux components is limited to just the productive part. Because of the flux balance conditions, futile fluxes are eliminated also from all other reactions that form part of the cycle.

FATMIN is a pipelined algorithm comprising FBA and flux variability analysis (FVA)[20] and therefore can be performed with either COBRA or OptFlux according to users' preference. The maximum reducing equivalent production rates for arbitrary growth rates between the data points were calculated using the interpolation function in Mathematica 8.0 (Wolfram Research, Inc). All the FBA and FATMIN results are detailed in the **Supplemental Tables.**

Disclosure of Potential Conflicts of Interest

No potential conflict of interest was disclosed.

Supplemental Materials

Supplemental materials may be found here:
www.landesbioscience.com/journals/bioe/articles/26222

References

1. Dequin S, Casaregola S. The genomes of fermentative *Saccharomyces.* C R Biol 2011; 334:687-93; PMID:21819951; http://dx.doi.org/10.1016/j.crvi.2011.05.019

2. Gibbs PEM, Wang X-D, Li Z, McManus TP, McGregor WG, Lawrence CW, Maher VM. The function of the human homolog of *Saccharomyces cerevisiae* REV1 is required for mutagenesis induced by UV light. Proc Natl Acad Sci U S A 2000; 97:4186-91; PMID:10760286; http://dx.doi.org/10.1073/pnas.97.8.4186

3. Reenan RA, Kolodner RD. Isolation and characterization of two *Saccharomyces cerevisiae* genes encoding homologs of the bacterial HexA and MutS mismatch repair proteins. Genetics 1992; 132:963-73; PMID:1459447

4. Garcerá A, Martínez AI, Castillo L, Elorza MV, Sentandreu R, Valentín E. Identification and study of a *Candida albicans* protein homologous to *Saccharomyces cerevisiae* Ssr1p, an internal cell-wall protein. Microbiology 2003; 149:2137-45; PMID:12904553; http://dx.doi.org/10.1099/mic.0.26301-0

5. Freire R, Murguía JR, Tarsounas M, Lowndes NF, Moens PB, Jackson SP. Human and mouse homologs of Schizosaccharomyces pombe rad1(+) and Saccharomyces cerevisiae RAD17: linkage to checkpoint control and mammalian meiosis. Genes Dev 1998; 12:2560-73; PMID:9716408; http://dx.doi.org/10.1101/gad.12.16.2560

6. Karathia H, Vilaprinyo E, Sorribas A, Alves R. *Saccharomyces cerevisiae* as a model organism: a comparative study. PLoS One 2011; 6:e16015; PMID:21311596; http://dx.doi.org/10.1371/journal.pone.0016015

7. Peralta-Yahya PP, Keasling JD. Advanced biofuel production in microbes. Biotechnol J 2010; 5:147-62; PMID:20084640; http://dx.doi.org/10.1002/biot.200900220

8. Rabaey K, Verstraete W. Microbial fuel cells: novel biotechnology for energy generation. Trends Biotechnol 2005; 23:291-8; PMID:15922081; http://dx.doi.org/10.1016/j.tibtech.2005.04.008

9. Babanova S, Hubenova Y, Mitov M. Influence of artificial mediators on yeast-based fuel cell performance. J Biosci Bioeng 2011; 112:379-87; PMID:21782506; http://dx.doi.org/10.1016/j.jbiosc.2011.06.008

10. Bullen RA, Arnot TC, Lakeman JB, Walsh FC. Biofuel cells and their development. Biosens Bioelectron 2006; 21:2015-45; PMID:16569499; http://dx.doi.org/10.1016/j.bios.2006.01.030

11. Mao L, Verwoerd W. Selection of organisms for systems biology study of microbial electricity generation: a review. International Journal of Energy and Environmental Engineering 2013; 4:17; http://dx.doi.org/10.1186/2251-6832-4-17

12. Logan BE, Hamelers B, Rozendal R, Schröder U, Keller J, Freguia S, Aelterman P, Verstraete W, Rabaey K. Microbial fuel cells: methodology and technology. Environ Sci Technol 2006; 40:5181-92; PMID:16999087; http://dx.doi.org/10.1021/es0605016

13. Heiskanen A, Spégel C, Kostesha N, Lindahl S, Ruzgas T, Emnéus J. Mediator-assisted simultaneous probing of cytosolic and mitochondrial redox activity in living cells. Anal Biochem 2009; 384:11-9; PMID:18812160; http://dx.doi.org/10.1016/j.ab.2008.08.030

14. Sayed ET, Tsujiguchi T, Nakagawa N. Catalytic activity of baker's yeast in a mediatorless microbial fuel cell. Bioelectrochemistry 2012; 86:97-101; PMID:22357359; http://dx.doi.org/10.1016/j.bioelechem.2012.02.001

15. Gunawardena A, Fernando S, To F. Performance of a yeast-mediated biological fuel cell. Int J Mol Sci 2008; 9:1893-907; PMID:19325724; http://dx.doi.org/10.3390/ijms9101893

16. Raghavulu SV, Goud RK, Sarma PN, Mohan SV. Saccharomyces cerevisiae as anodic biocatalyst for power generation in biofuel cell: influence of redox condition and substrate load. Bioresour Technol 2011; 102:2751-7; PMID:21146401; http://dx.doi.org/10.1016/j.biortech.2010.11.048

17. Oberhardt MA, Palsson BO, Papin JA. Applications of genome-scale metabolic reconstructions. Mol Syst Biol 2009; 5:320; PMID:19888215; http://dx.doi.org/10.1038/msb.2009.77

18. Lewis NE, Nagarajan H, Palsson BO. Constraining the metabolic genotype-phenotype relationship using a phylogeny of in silico methods. Nat Rev Microbiol 2012; 10:291-305; PMID:22367118

19. Mao L, Verwoerd WS. Genome-scale stoichiometry analysis to elucidate the innate capability of the cyanobacterium *Synechocystis* for electricity generation. J Ind Microbiol Biotechnol 2013; PMID:23851491; http://dx.doi.org/10.1007/s10295-013-1308-0

20. Mao L, Verwoerd WS. Model-driven elucidation of the inherent capacity of Geobacter sulfurreducens for electricity generation. J Biol Eng 2013; 7:14; PMID:23718629; http://dx.doi.org/10.1186/1754-1611-7-14

21. Heavner BD, Smallbone K, Barker B, Mendes P, Walker LP. Yeast 5 - an expanded reconstruction of the *Saccharomyces cerevisiae* metabolic network. BMC Syst Biol 2012; 6:55; PMID:22663945; http://dx.doi.org/10.1186/1752-0509-6-55

22. Mao L, Verwoerd WS. Computational comparison of mediated MFC current generation capacity of Chlamydomonas reinhardtii in photosynthetic and respiratory growth modes. In press.

23. Cheetham NWH. Introducing Biological Energetics: How Energy and Information Control the Living World New York: Oxford University Press, 2011.

24. Kim BH, Park HS, Kim HJ, Kim GT, Chang IS, Lee J, Phung NT. Enrichment of microbial community generating electricity using a fuel-cell-type electrochemical cell. Appl Microbiol Biotechnol 2004; 63:672-81; PMID:12908088; http://dx.doi.org/10.1007/s00253-003-1412-6

25. Haslett ND, Rawson FJ, Barrière F, Kunze G, Pasco N, Gooneratne R, Baronian KHR. Characterisation of yeast microbial fuel cell with the yeast Arxula adeninivorans as the biocatalyst. Biosens Bioelectron 2011; 26:3742-7; PMID:21493057; http://dx.doi.org/10.1016/j.bios.2011.02.011

26. Ganguli R, Dunn BS. Kinetics of Anode Reactions for a Yeast-Catalysed Microbial Fuel Cell. Fuel Cells (Weinh) 2009; 9:44-52; http://dx.doi.org/10.1002/fuce.200800039

27. Videla HA, Arvía AJ. The response of a bioelectro-chemical cell with Saccharomyces cerevisiae metaboliz-ing glucose under various fermentation conditions. Biotechnol Bioeng 1975; 17:1529-43; PMID:241440; http://dx.doi.org/10.1002/bit.260171011

28. Park DH, Kim SK, Shin IH, Jeong YJ. Electricity pro-duction in biofuel cell using modified graphite electrode with Neutral Red. Biotechnol Lett 2000; 22:1301-4; http://dx.doi.org/10.1023/A:1005674107841

29. Park DH, Zeikus JG. Electricity generation in micro-bial fuel cells using neutral red as an electrono-phore. Appl Environ Microbiol 2000; 66:1292-7; PMID:10742202; http://dx.doi.org/10.1128/AEM.66.4.1292-1297.2000

30. Jeong H, Tombor B, Albert R, Oltvai ZN, Barabási AL. The large-scale organization of metabolic networks. Nature 2000; 407:651-4; PMID:11034217; http://dx.doi.org/10.1038/35036627

31. Famili I, Förster J, Nielsen J, Palsson BO. *Saccharomyces cerevisiae* phenotypes can be predicted by using con-straint-based analysis of a genome-scale reconstruct-ed metabolic network. Proc Natl Acad Sci U S A 2003; 100:13134-9; PMID:14578455; http://dx.doi.org/10.1073/pnas.2235812100

32. Edwards JS, Ibarra RU, Palsson BO. In silico predic-tions of Escherichia coli metabolic capabilities are consistent with experimental data. Nat Biotechnol 2001; 19:125-30; PMID:11175725; http://dx.doi.org/10.1038/84379

33. Fong SS, Palsson BO. Metabolic gene-deletion strains of Escherichia coli evolve to computationally predicted growth phenotypes. Nat Genet 2004; 36:1056-8; PMID:15448692; http://dx.doi.org/10.1038/ng1432

34. Varma A, Palsson BO. Stoichiometric flux balance models quantitatively predict growth and metabolic by-product secretion in wild-type Escherichia coli W3110. Appl Environ Microbiol 1994; 60:3724-31; PMID:7986045

35. Ibarra RU, Edwards JS, Palsson BO. Escherichia coli K-12 undergoes adaptive evolution to achieve in silico predicted optimal growth. Nature 2002; 420:186-9; PMID:12432395; http://dx.doi.org/10.1038/nature01149

36. Burgard AP, Maranas CD. Optimization-based frame-work for inferring and testing hypothesized metabolic objective functions. Biotechnol Bioeng 2003; 82:670-7; PMID:12673766; http://dx.doi.org/10.1002/bit.10617

37. Pereyra V, Saunders M, Castillo J. Equispaced Pareto front construction for constrained bi-objective opti-mization. Math Comput Model 2013; 57:2122-31; http://dx.doi.org/10.1016/j.mcm.2010.12.044

38. Ekins S, Honeycutt JD, Metz JT. Evolving mol-ecules using multi-objective optimization: applying to ADME/Tox. Drug Discov Today 2010; 15:451-60; PMID:20438859; http://dx.doi.org/10.1016/j.drudis.2010.04.003

39. Kim K-Y, Chae K-J, Choi M-J, Ajayi FF, Jang A, Kim C-W, Kim IS. Enhanced Coulombic efficiency in glucose-fed microbial fuel cells by reducing metabolite electron losses using dual-anode electrodes. Bioresour Technol 2011; 102:4144-9; PMID:21216140; http://dx.doi.org/10.1016/j.biortech.2010.12.036

40. Suthers PF, Zomorrodi A, Maranas CD. Genome-scale gene/reaction essentiality and synthetic lethality analysis. Mol Syst Biol 2009; 5:301; PMID:19690570; http://dx.doi.org/10.1038/msb.2009.56

41. Zomorrodi AR, Maranas CD. Improving the iMM904 *S. cerevisiae* metabolic model using essentiality and synthetic lethality data. BMC Syst Biol 2010; 4:178; PMID:21190580; http://dx.doi.org/10.1186/1752-0509-4-178

42. Schellenberger J, Que R, Fleming RM, Thiele I, Orth JD, Feist AM, Zielinski DC, Bordbar A, Lewis NE, Rahmanian S, et al. Quantitative prediction of cellular metabolism with constraint-based models: the COBRA Toolbox v2.0. Nat Protoc 2011; 6:1290-307; PMID:21886097; http://dx.doi.org/10.1038/nprot.2011.308

43. Mo ML, Palsson BO, Herrgård MJ. Connecting extracellular metabolomic measurements to intracel-lular flux states in yeast. BMC Syst Biol 2009; 3:37; PMID:19321003; http://dx.doi.org/10.1186/1752-0509-3-37

44. Varma A, Palsson BO. Metabolic Flux Balancing: Basic Concepts, Scientific and Practical Use. Nat Biotechnol 1994; 12:994-8; http://dx.doi.org/10.1038/nbt1094-994

45. Orth JD, Thiele I, Palsson BO. What is flux bal-ance analysis? Nat Biotechnol 2010; 28:245-8; PMID:20212490; http://dx.doi.org/10.1038/nbt.1614

46. Rocha I, Maia P, Evangelista P, Vilaça P, Soares S, Pinto JP, Nielsen J, Patil KR, Ferreira EC, Rocha M. OptFlux: an open-source software platform for in silico metabolic engineering. BMC Syst Biol 2010; 4:45; PMID:20403172; http://dx.doi.org/10.1186/1752-0509-4-45

47. Virdis B, Freguia S, Rozendal RA, Rabaey K, Yuan Z, Keller J. 4.18 - Microbial Fuel Cells. In: Editor-in-Chief: Peter W, ed. Treatise on Water Science. Oxford: Elsevier, 2011:641-65.

48. Cheng S, Liu H, Logan BE. Increased power gen-eration in a continuous flow MFC with advective flow through the porous anode and reduced elec-trode spacing. Environ Sci Technol 2006; 40:2426-32; PMID:16646485; http://dx.doi.org/10.1021/es051652w

49. Zhao F, Harnisch F, Schröder U, Scholz F, Bogdanoff P, Herrmann I. Challenges and constraints of using oxygen cathodes in microbial fuel cells. Environ Sci Technol 2006; 40:5193-9; PMID:16999088; http://dx.doi.org/10.1021/es060332p

50. Schröder U. Anodic electron transfer mechanisms in microbial fuel cells and their energy efficiency. Phys Chem Chem Phys 2007; 9:2619-29; PMID:17627307; http://dx.doi.org/10.1039/b703627m